Zhang et al. *NPG Asia Materials* (2022)14:50
https://doi.org/10.1038/s41427-022-00396-2

NPG Asia Materials

ARTICLE Open Access

Atomic origin of the coexistence of high critical current density and high T_c in $CuBa_2Ca_3Cu_4O_{10+\delta}$ superconductors

Xuefeng Zhang[1,2], Jianfa Zhao[3], Huijuan Zhao[1,2], Luchuan Shi[3], Sihao Deng[4], Jie Chen[4], Lunhua He[4], Zhiwei Hu[5], Changqing Jin[3] and Jing Zhu[1,2]

Abstract

For cuprate superconductors, a high critical transition temperature (T_c) can be realized in compounds containing multiple CuO_2 layers in the unit cell, while a high critical current density (J_c) is rarely sustained above liquid nitrogen temperature. The $CuBa_2Ca_3Cu_4O_{10+\delta}$ (Cu-1234) superconductors synthesized under high oxygen pressure incredibly exhibit high T_c (~117 K) and high J_c (>10^4 A/cm^2, 100 K) values. Here, the "double high" traits of Cu-1234 were investigated with advanced scanning transmission electron microscopy. It was revealed that ordering vacancies and plate-like 90° microdomains induced efficient microstructure pinning centers that suppressed vortex flux flow and enhanced J_c. Furthermore, metallic charge-reservoir blocks [$Ba_2CuO_{3+\delta}$] were composed of unique compressed [CuO_6] octahedra, which induced many holes with $2p_z$ symmetry that significantly decreased the superconducting anisotropy and dramatically enhanced the interlayer coupling that guaranteed a high J_c. On the other hand, optimally doped CuO_2 planes inside the thick superconducting blocks [$Ca_3Cu_4O_8$] maintained a high T_c. Our results are applicable to design and synthesis of new superconductors with "double high" traits.

Introduction

Critical-current density (J_c) is a parameter of primary importance for potential applications of high-temperature superconductors (HTSCs), and it is limited principally by breakdown of zero-resistive current due to thermally activated flux flow under high temperature and high magnetic fields[1,2]. The "intrinsic" J_c at liquid nitrogen temperature is limited by the strong two-dimensional (2D) anisotropy of HTSCs, as well as the short coherence length, which is unfavorable for vortex pinning[3–5]. Among cuprate superconductors, application of Bi-based compounds at liquid nitrogen temperature is primarily limited by sharp decreases in J_c values due to the strong anisotropy[6,7]. For Tl- and Hg-based compounds, the high anisotropy as well as the toxic Tl and Hg elements constrain applications[8,9]. Furthermore, the nontoxic $YBa_2Cu_3O_{7-\delta}$ (YBCO) superconductor with relatively low anisotropy (γ~5), which has a high T_c (~90 K) and a high J_c (å 10^4 A/cm^2 at 77 K), is best in terms of comprehensive properties[10,11]. The absolute value of J_c is also determined extrinsically by the microstructure, which introduces efficient pinning centers into crystals suppressing the flux flow[4,12–15]. It has already been shown that overdoping HTSCs is effective in decreasing the anisotropies of HTSCs and increasing the irreversibility fields (H_{irr})[5,16,17]. However, the T_c values drop drastically with increasing carrier concentration in the overdoped region. The trade-off between T_c and J_c or H_{irr} in the overdoped region is a crucial problem for HTSCs.

Cu-1234 is a heavily overdoped superconductor that belongs to the $CuBa_2Ca_{n-1}Cu_nO_{2n+2+\delta}$ ($n = 2, 3, 4...$)

Correspondence: Changqing Jin (Jin@iphy.ac.cn) or
Jing Zhu (jzhu@mail.tsinghua.edu.cn)
[1]National Center for Electron Microscopy in Beijing, School of Materials Science and Engineering, Key Laboratory of Advanced Materials (MOE), The State Key Laboratory of New Ceramics and Fine Processing, Tsinghua University, Beijing 100084, China
[2]Ji Hua Laboratory, Foshan 528299, China
Full list of author information is available at the end of the article

family. In previous studies, Cu-1234 has been reported to have the following features: (I) a high T_c above 117 K at ambient pressure near that of Hg-1223, which has the highest T_c in cuprates; (II) excellent critical current densities at liquid nitrogen temperature, which are superior to Bi cuprate homologous superconductors and comparable to the classical Y-based system[18,19]. The persistent J_c(T) relative to its value at absolute zero decreases roughly exponentially as $\exp(-T/T_0)$ because of flux creep[20]. The values of T_0 reported are ~7 and 4–5 K for Hg systems and Bi-2212, respectively, which caused the J_c values to drop rapidly to near zero at liquid nitrogen temperature[6,8,20]. While the values of T_0 reported to date were 16–20 K and ~23 K for Cu-1234 and YBCO, respectively, the values of J_c for both reached $>10^4$ A/cm^2 at 77 K[10,19–21]; and (III) it contains alkaline earth copper oxides only but is stable in air[19]. However, the origin of this excellent superconducting behavior in Cu-1234, especially the high J_c above liquid nitrogen temperature, has rarely been reported and is not understood. In this paper, we report systematic studies on the lattice and electronic structure of Cu-1234 by using Cs-corrected STEM combined with neutron powder diffraction (NPD) and X-ray adsorption spectroscopy (XAS) and reveal the interaction between lattice and charge that may be intimately related to the excellent "double high" performance of Cu-1234. Our results are applicable to design and synthesis of new multilayered superconductors with high T_c as well as high J_c.

Materials and methods

The Cu-1234 sample was synthesized by a solid-state reaction method under high pressure and high temperature conditions. The detailed experimental procedure is described in the literature[18]. The starting materials were CaO (99.95% pure, Alfa Aesar), CuO (99.995% pure, Alfa Aesar), and BaO_2 (95% pure, Alfa Aesar). All of the operations were performed under argon gas in a glove box with oxygen and vapor levels of less than 1 ppm due to the highly hygroscopic nature of alkaline-earth metallic oxides. High-pressure experiments were performed with a cubic anvil-type high-pressure apparatus. After the pressure was gradually increased to 6 GPa, the sample was heated to 1273 K and maintained there for 30 min. Then, the temperature was reduced to ambient before releasing the pressure. After the high-pressure and high-temperature process, the superconductive Cu-1234 sample was obtained. Cross-sectional TEM specimens were prepared by a standard procedure that included mechanical grinding, tripod polishing, and argon ion beam milling in a stage cooled with liquid nitrogen. The thickness of the sample was less than 20 nm.

Atomic scale structures of Cu-1234 samples were studied by using a combination of selected area electron diffraction and high-angle annular dark field (HAADF) and annular bright field (ABF) imaging methods. Aberration-corrected STEM studies were performed on an FEI Titan Cubed Themis 60–300 (operating at 300 kV), which was capable of recording high-resolution STEM images with a spatial resolution of ≈ 0.06 nm. The microscopy equipment included a high brightness electron gun (X-FEG with a monochromator), a C_S probe corrector, a C_S image corrector, and a postcolumn imaging energy filter (Gatan Quantum 965 Spectrometer). ABF and HAADF images were acquired at acceptance angles of 12–45 and 64–200 mrad, respectively. The SI data and the ADF signal in the STEM-EELS experiments were simultaneously acquired with a beam current of ~40 to 50 pA, a convergence semiangle of 25 mrad, a GIF collection semiangle of 55 mrad, and a pixel dwell time of 25 ms to maximize the signal while minimizing drift and beam damage artifacts. The orientation-dependent EELS measurements for the O-*K* edge in the TEM diffraction mode used a GIF collection semiangle of 0.362 mrad, an entrance aperture of 2.5 mm and a total sum time of 50 s to maximize the signal. NPD studies were performed on a GPPD (general purpose powder diffractometer) time-of-flight diffractometer at the CSNS (China Spallation Neutron Source), Dongguan, China. The obtained NPD data were analyzed by the Rietveld method with the GSAS/EXPGUI package[22]. The magnetic properties of the sample were measured using a superconducting quantum interference device magnetometer (Quantum Design MPMS3-7T). The magnetization hysteresis loop was measured with a Cu-1234 powder sample. The Cu-1234 sample was finely ground and sealed in a nonmagnetic capsule. Soft X-ray absorption spectroscopy (XAS) at the O-*K* edge was measured at the BL08B beamline of the National Synchrotron Radiation Research Center (NSRRC) in Taiwan.

Results and discussion

The Cu-1234 bulk sample was synthesized via a solid-state reaction run under high pressure and high temperature conditions[18,19,23]. The NPD measurements demonstrated that these samples, in general, had a tetragonal basic structure with lattice parameters $a = b = 3.85856(5)$ Å, $c = 17.9544(6)$ Å, and space group of $P4/mmm$ (No. 123). This structure is similar to the crystal structure of the 1234 phase known for Tl-based or Hg-based superconducting systems, such as $HgBa_2Ca_3Cu_4O_{10+\delta}$[24] and $TlBa_2Ca_3Cu_4O_{10+\delta}$[25]. The actual chemical composition of Cu-1234 based on NPD refinement was $Cu_{0.94}Ba_2Ca_3Cu_4O_{10.66}$, which indicated that the average valence state of Cu was +2.29 (more details on the refined structural parameters are listed in Table S1). As shown in Fig. 1a, Ba1, Cu1, O1, and O2 formed charge reservoir blocks [$Ba_2CuO_{3+\delta}$] (CRBs), while Cu2, Cu3, Ca1, Ca2, O3, and O4 formed superconducting blocks [$Ca_3Cu_4O_8$] (SCBs). The number of

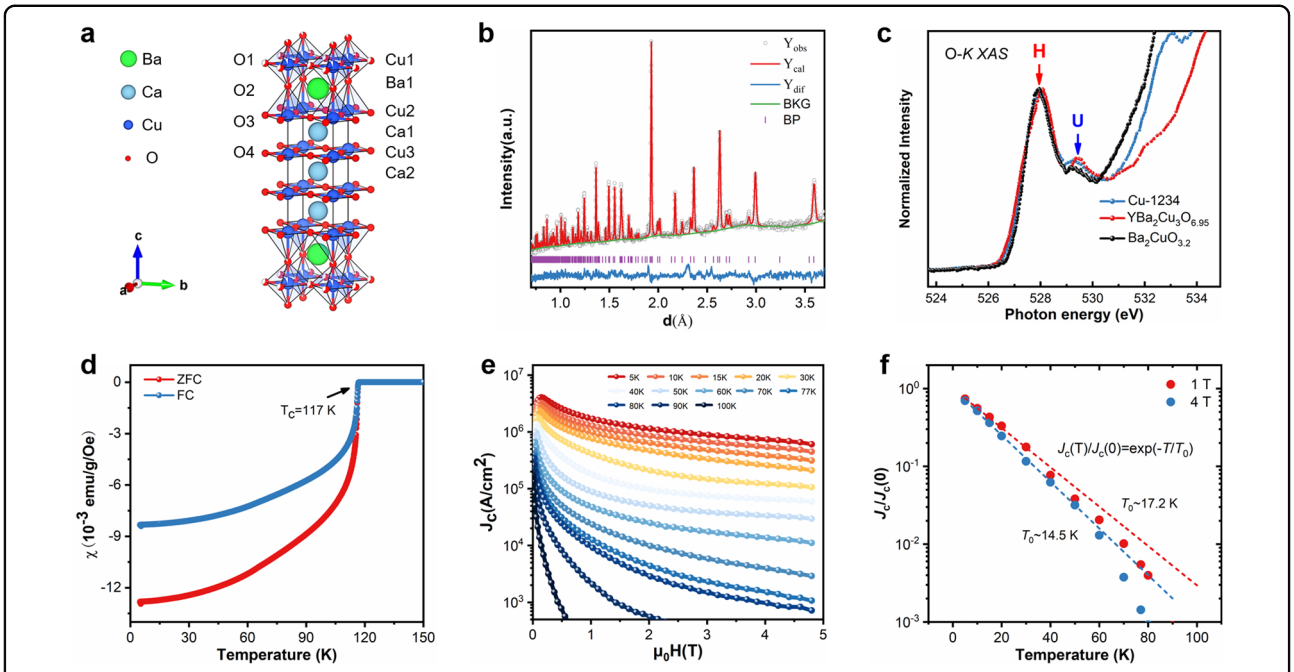

Fig. 1 Crystal structure and superconducting properties of Cu-1234. a Crystal structure of Cu-1234 based on NPD data. The Cu1, O1, and O2 sites are partially occupied, and the occupancy ratios are 0.94, 0.54, and 0.79, respectively. **b** Rietveld refinements for Cu-1234 based on NPD data obtained at 300 K. Observed (crosses), calculated (red), and difference (blue) values are shown in the figure. **c** O-*K* XAS spectra of Cu-1234 shown together with those for overdoped $YBa_2Cu^{2.30+}{}_3O_{6.95}$[29] and $Ba_2Cu^{2.40+}O_{3.2}$[30] as references. **d** Temperature dependence of the magnetic susceptibility of Cu-1234 measured in the ZFC and FC modes with an applied field of 30 Oe. The transition temperature is approximately 117 K. **e** Field dependence of the critical current density J_c at various temperatures. J_c is determined by the formula $J_c(A/cm^2) = 30\Delta M/d$, where d is the average grain size of the powdered sample, and the averaged grain size d is 10 μm according to the SEM image (Fig. S3). **f** Normalized critical current density $J_c(T)/J_c(0)$ at 1 T (red) and 4 T (blue) as a function of temperature. Roughly, $J_c(T) = J_c(0)\exp(-T/T_0)$ behavior appears below 60 K. The two straight lines are the fitting lines at 1 T (red) and 4 T (blue).

doped holes was quantitatively characterized by the O-*K* XAS spectrum shown in Fig. 1c[26–28]. Peaks H and U are attributed to transitions from O 1*s* to the doped hole states and upper Hubbard band, respectively. The spectral weight of U in Cu-1234 was weaker than that in $YBa_2Cu^{2.30+}{}_3O_{6.95}$[29] but slightly higher than that of $Ba_2Cu^{2.40+}O_{3.2}$[30], indicating that the doping level in Cu-1234 was slightly smaller than that of $Ba_2Cu^{2.40+}O_{3.2}$ but higher than that of $YBa_2Cu^{2.30+}{}_3O_{6.95}$; this confirmed the overdoped nature of Cu-1234. The superconducting transition occurred at 117 K, as indicated by the magnetization measurement (Fig. 1d). The critical current densities J_c versus magnetic field at different temperatures were calculated from magnetic hysteresis loops (Fig. S1) by using the Bean model, and these are plotted in Fig. 1e. The values of J_c for Cu-1234 were approximately 5.6×10^5 A/cm^2 (77 K) in the Earth's field, which are much larger than those of Bi, Hg-, and Tl-based cuprate superconductors and comparable to that of YBCO at liquid nitrogen temperatures[19]. The J_c of Cu-1234 in this work reached approximately 1.7×10^5 A/cm^2 (100 K), which provides great potential for high-power applications in the temperature range near 100 K. The temperature dependence of J_c at 1 and 4 T was normalized against $J_c(0)$ and is shown in Fig. 1f. The data from 5 to 60 K fit the relation $J_c(T) = J_c(0)\exp(-T/T_0)$, and the fitting parameters T_0 at 1 and 4 T were 17.16 ± 0.45 and 14.49 ± 0.28 K, respectively. The T_0 values for the Y-123 and Hg systems (Hg-1201, Hg-1212, and Hg-1223) and Bi-2212 were 20–23, ~7, and 4–5 K, respectively[20,31]. T_0 for the as-synthesized sample in this study (~17.2 K) was relatively large and close to that of Y-123, which can be attributed to the similarity of the CRBs of Cu-1234 and Y-123. The large value of J_c and its weak dependence on field and temperature all suggested strong flux pinning by Cu-1234.

Ordering of the copper and oxygen vacancies was discovered to exhibit an $\boldsymbol{a}\times 2\boldsymbol{b}\times 2\boldsymbol{c}$ modulated structure and induce periodic lattice distortions in Cu-1234. As shown in Fig. 2a, the copper and oxygen vacancies were situated at Cu1a, O1a, and O2a sites, while the Cu1b, O1b, and O2b sites were fully occupied, resulting in doubling of the ***b*** axis and a loss of tetragonal symmetry. Specifically, the corresponding HAADF and ABF images were taken along the [100] zone axis. In Fig. 2b, due to the copper and

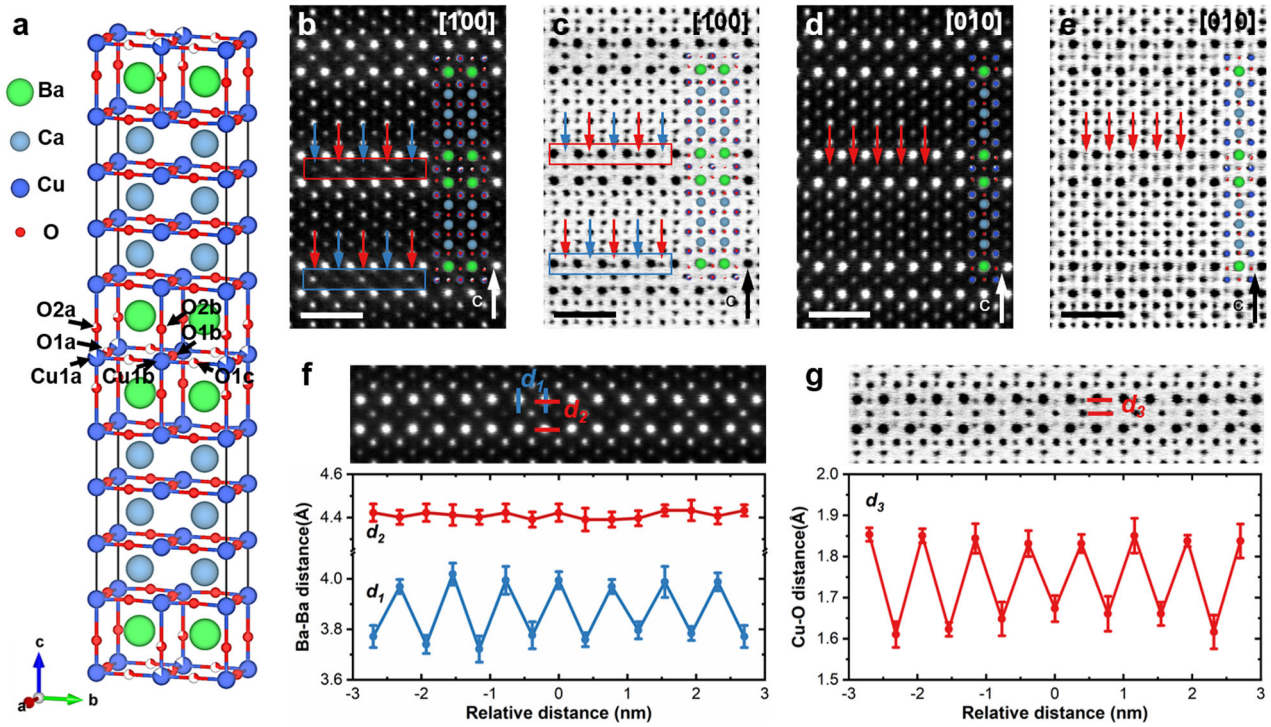

Fig. 2 Vacancy ordering and periodic lattice distortions induced in Cu-1234. a Crystal structure of Cu-1234 with an *a*×2*b*×2*c* modulated structure. **b**, **c** Atomic resolved HAADF-STEM and ABF-STEM images of Cu-1234 taken along the [100] zone axis, respectively. The red and blue arrows illustrate the relatively bright and dark intensities of the Cu1bO1b column and Cu1aO1a column, respectively. Scale bar = 1 nm. **d**, **e** Atomic resolved HAADF-STEM and ABF-STEM images of Cu-1234 taken along the [010] zone axis, respectively. Scale bar = 1 nm. **f** Ba–Ba atomic column spacings along the in-plane (d_1) and out-of-plane (d_2) directions as a function of the relative distance between Cu sites. **g** O–Cu atomic column distance along the out-of-plane (d_3) direction as a function of the relative distance of Cu sites.

oxygen vacancies in Cu1a and O1a sites, Cu1a(O1a) columns showed much weaker intensity than those of Cu1b (O1b). The arrangement of atomic columns in the red frame is -Cu1aO1a (overlap)-Cu1bO1b (overlap)-Cu1aO1a (overlap)-, which gives 2***b*** periodicity, as clearly illustrated by blue and red arrows. The arrangement of atomic columns in the blue frame is different: -Cu1bO1b (overlap)-Cu1aO1a (overlap)-Cu1bO1b (overlap)-, resulting in 2***c*** periodicity in the modulated structure. In Fig. 2c, the intensity of O2 sites in BaO layers also shows 2***b*** and 2***c*** periodicity. Our ***a***×2***b***×2***c*** modulated structural model for Cu-1234 with the *Ammm* space group was also confirmed by the corresponding HAADF and ABF images taken along the [010] zone axis. In Fig. 2d, the overlapping Cu1a(O1a) and Cu1b(O1b) columns display nearly the same intensity; this indicates disordered vacancies at Cu1aO1a sites along the [100] direction, as illustrated by red arrows. Similarly, in Fig. 2e, the oxygen vacancies at O2a sites were disordered along the [100] directions. Figure 2f, g shows the variations in Ba–Ba spacing and O–Cu spacing for each CRB along the [010] direction. The values of the in-plane (d_1) Ba–Ba atomic distances at deficient [$Ba_2Cu1aO_{3+\delta}$] sites were larger than those of d_1 at perfect Cu1b sites, so the values of for out-of-plane (d_3) Cu–O distances were opposite. These alternately occurring maximum and minimum values indicated periodic lattice distortions, which was induced by vacancy ordering and was consistent with the 2***b*** periodicity mentioned above. Varying the Cu–O bond length would profoundly modify the pairing landscape by producing regions of either enhanced or depressed pairing, which is required to induce vortex pinning[16,32] (electron diffraction patterns and structural parameters of Cu-1234 with an ***a***×2***b***×2***c*** modulated structure are shown in Fig. S2 and Table S2, respectively).

As further demonstrated by the dark-field experiments and STEM experiments, we also found that the crystal can form 90° microdomains in the above mentioned ***a***×2***b***×2***c*** modulated structure. Figure 3a displays thin, platelike domains, with longitudinal dimensions varying from 100 to 500 nm and transverse dimensions along the *c* axis ranging from 2 to 50 nm. The area showing bright contrast is along the [100] zone axis, while the area showing dark contrast is along the [010] zone axis. The atomic structure of the 90° microdomains is shown in Fig. 3b, where their *c*-axes are parallel while their *a*-axes are

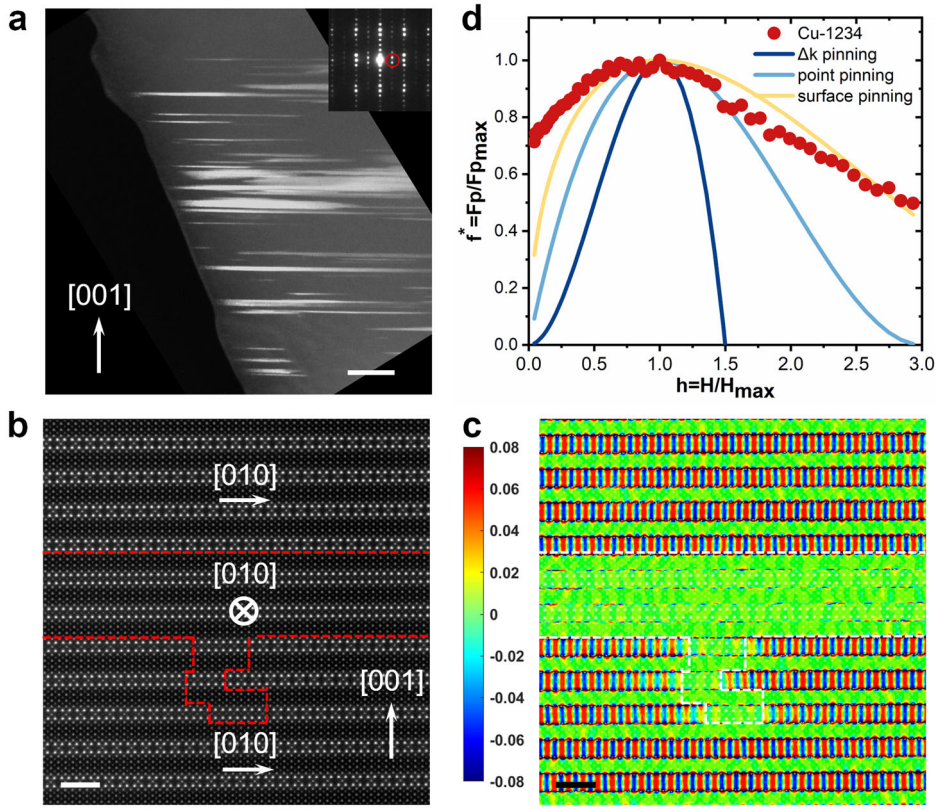

Fig. 3 Thin, plate-like 90° microdomains and flux pinning mechanism for Cu-1234. a Dark-field image of Cu-1234 using electrons scattered from the superstructure spots circled in the inset. Scale bar = 100 nm. **b** Atomic resolved HAADF-STEM image of plate-like microdomains in (**a**), where their *c*-axes are parallel and their *a*-axes are perpendicular to each other. Scale bar = 2 nm. **c** Strain mappings of e_{xx} derived from the HAADF-STEM image in (b by GPA and overlaid on the HAADF-STEM image. Here, the *x* directions are parallel to the *b* axis. Scale bar = 2 nm. **d** Plots of the normalized pinning force $f^* = F_p/F_{pmax}$ vs. $h = H/H_{max}$. The pinning force $F_p(H)$ ($F_p(H) = J_c(H) \times H$) data were rescaled by $h^* = H/H_{max}$ (H_{max} is the magnetic field when F_p reaches the maximum). Scaling of the $f^*(h)$ data can be determined with the following equations: $1/3f^*(h) = h^2(1 - 2h/3)$ (for $\Delta\kappa$ pinning), $4/9f^*(h) = h(1 - h/3)^2$ (for normal point pinning), $16/25f^*(h) = h^{1/2}(1 - h/5)^2$ (for surface pinning).

perpendicular to each other. The local strain states between domains were further explored by geometrical phase analysis (GPA)[33,34] carried out on the HAADF-STEM image shown in Fig. 3b. Figure 3c shows the mapping of the in-plane deformation (e_{xx}, along the [010] direction). The ordered copper and oxygen vacancies in CRBs along the [010] direction show periodic tensile and compressive strain, while the disordered vacancies along the [100] direction show no periodicity. Similar to the twin boundaries in YBCO[13,35] or domains in heavily Pb-doped $Bi_2Sr_2CaCu_2O_{8+\delta}$, these thin, plate-like microdomains in Cu-1234 are believed to disturb flux flow and increase J_c[4] since electron scattering at the boundaries may reduce the coherence length locally. Furthermore, we systematically studied the flux pinning force at 77 K and compared it with surface pinning, $\Delta\kappa$ pinning, and normal point pinning[36,37], as shown in Fig. 3d. It is obvious that the experimental data followed the case of surface pinning well, demonstrating that the actual dominant pinning centers are surface pinning centers. Such correlated defects, including vacancy ordering and 90° microdomains in Cu-1234, are believed to suppress the thermal fluctuations of vortices more efficiently than randomly distributed point defects.

The "intrinsic" high-J_c seen at liquid nitrogen temperature for heavily overdoped Cu-1234 originated from its special composition and crystal structure. As shown in Fig. 4a, Cu-1234 consists of thick (0.96 nm) superconducting blocks [$Ca_3Cu_4O_8$] (SCBs) with four CuO_2 planes and metallic conductive charge reservoir blocks [$Ba_2CuO_{3+\delta}$] (CRBs) with CuO_6 octahedra. The SCBs included two crystallographically inequivalent CuO_2 planes, the outer CuO_2 planes in pyramidal clusters (OPs) with apical oxygen and inner square CuO_2 planes (IPs) without apical oxygen. The in-plane and out-of-plane Cu-O bond lengths in CRBs were 1.929(3) Å and 1.777(5) Å, respectively. This yielded exceptionally compressed CuO_6 local octahedra in the CRBs. The crystal structure

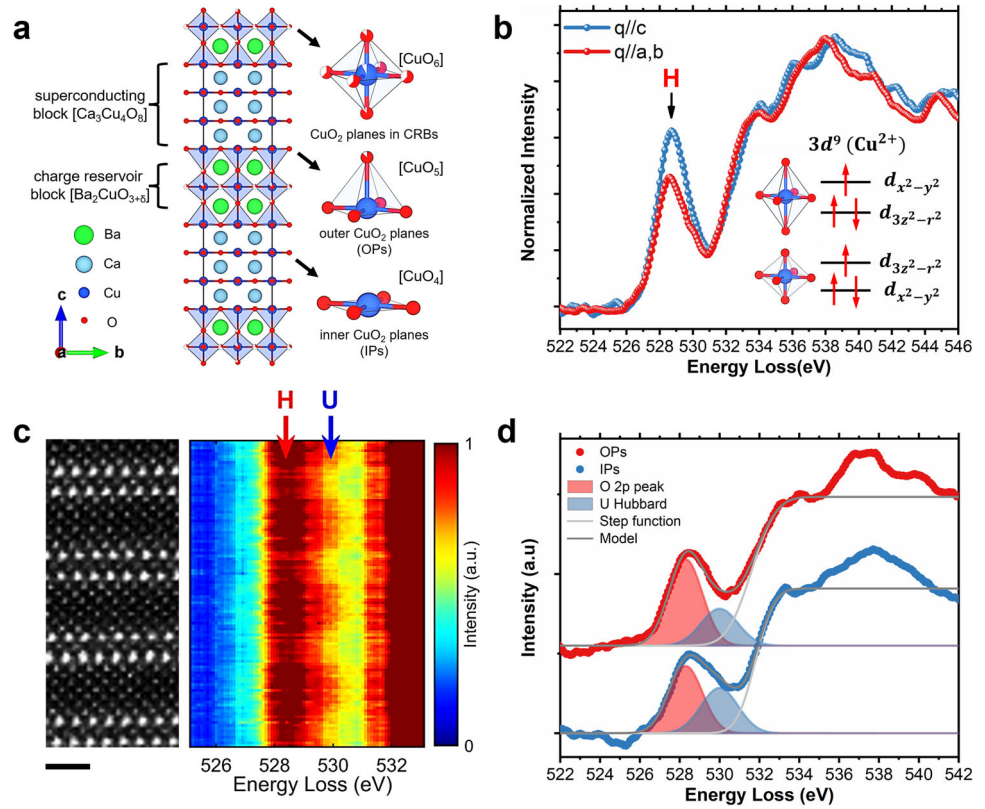

Fig. 4 Symmetry and inhomogeneous distribution of holes in Cu-1234. a The atomic structural model of Cu-1234 with an *a*×2*b*×2*c* modulated structure. **b** O*1s* absorption edges of Cu-1234 for momentum transfer parallel to the *c* axis (blue) and in the *a,b* plane (red). The inset indicates the schematic crystal structure with an elongated "[CuO_6] octahedron", which pushes the $3d_{x2-y2}$ orbital energy level above the $3d_{3z2-r2}$ orbital energy level. However, in the compressed "[CuO6] octahedron", the $3d_{3z2-r2}$ orbital energy level is expected to be located above the $3d_{x2-y2}$ orbital energy level. **c** Spatially resolved EELS for Cu-1234 at the O-*K* edge. These spectra were integrated over the (*ab*) atomic planes but spatially resolved along the *c* axis, and intensity is displayed as a color scale. The positions of the O2*p* hole (H) and upper Hubbard (U) bands are indicated by red and black arrows, respectively. Weighted principal component analysis (PCA) was applied to reduce the noise level. Scale bar = 1 nm. **d** O-*K* edge EELS spectra obtained from OPs (red) and IPs (black). Two Gaussian functions were used to model the O2*p* hole band (red) and the upper Hubbard band (UHB) (blue). The background (gray solid lines) was modeled using a step function[43].

characteristics of Cu-1234 were similar to those of $Ba_2CuO_{3.2}$ (Ba-214), in which the in-plane and out-of-plane Cu–O bond lengths were 2.00 and 1.86 Å, respectively. We defined the compression ratio of the [CuO_6] local octahedron as $\sigma = d_{\text{out-of-plane}}/d_{\text{in-plane}}$, where $d_{\text{out-of-plane}}$ and $d_{\text{in-plane}}$ represent the out-of-plane and in-plane Cu–O bond lengths, respectively. According to this definition, the σ for CRBs in Cu-1234 is 0.92, which is very close to that for Ba-214 ($\sigma = 0.93$). In compressed octahedron, the energy of the $3d_{3z^2-r^2}$ orbital is lifted above that of the $3d_{x^2-y^2}$ orbital; this leads to significant doping holes in the unconventional $3d_{3z^2-r^2}$ orbital, which decrease the superconductivity anisotropy and enhances interlayer coupling. This deduction was further confirmed by orientation-dependent EELS measurements for the O 1*s* absorption edges, which probed the unoccupied electronic orbitals with 2*p* symmetry at O sites and their orientations with respect to the crystal axis. We recorded EELS data for the O-*K* edge using a relatively small collection semiangle (0.362 mrad), with the incident electron beam aligned along the *a-*, *b-*, and *c*-axes for *q//a, b,* and *q//c*, respectively. As shown in Fig. 4b, the prepeak at approximately 528.5 eV can be attributed to transitions from the O *1s* to O 2*p* states in the Zhang-Rice singlet band[29,38]. For *q//c* and *q//a, b*, a considerable number of holes having $2p_z$ and $2p_{x,y}$ symmetry were observed, respectively, and the former showed a higher hole concentration than the latter. This is significantly different from all other known cuprate superconductors[26,28,38–40], for which in-plane orbitals are unanimously predominant, indicating that the apical O $2p_z$ orbitals can play an important role in the intrinsic high-J_c.

The coexistence of high T_c (~117 K) and high carrier concentration (~0.29 hole/CuO_2) in Cu-1234 was investigated by STEM-EELS at atomic resolution and was due to the inhomogeneous carrier distribution among the

CuO_2 planes. Figure 4c presents spatially resolved O-*K* edge EELS spectra, which provide simple layer by layer visualization of changes in the fine structure. Obviously, the strong intensity of peak H appearing for CRBs indicates their metallic conductivity. A high carrier concentration existed in both SCBs and CRBs, which is essential for low superconducting anisotropy and high-J_c and high-H_{irr}[5]. Specifically, the O-*K* edge EELS spectra of OPs and IPs are shown in Fig. 4d. Compared with OPs, considerable spectral weight was transferred from the O 2*p* peak H (~528.5 eV) to the upper Hubbard peak U (~530 eV) in IPs. Since the spectral weight of this preedge depends on the doping level, OPs show much higher hole concentrations than IPs. The bond valence sum calculation (BVS)[41] based on NPD refinement (Table S3) provided additional evidence for an inhomogeneous hole distribution and showed valence states of +2.45 for Cu1, +2.14 for Cu2, and +2.03 for Cu3. The apical oxygen connects CRBs and SCBs and transfers holes from Cu ions to OPs, thereby enhancing the hole concentration in OPs. The difference in hole concentrations for OPs and IPs increases the average hole concentration, while the IPs maintain a near-optimal doping concentration to maintain T_c at approximately 117 K in the heavily overdoped region. Strong superconducting coupling between the thick SCBs mediated by CRBs and overdoped carriers contributes to the intrinsic high J_c of Cu-1234.

Although Cu-1234 shows both high-T_c and intrinsic intragrain high-J_c, the grain boundary has a detriment effect on the critical current density J_c of the polycrystalline bulk sample. Actually, the connectivity between grains of the polycrystalline bulk is strongly degraded due to grain boundaries with weak coupling. Therefore, the currents cannot circulate well over the bulk sample, which inhibits the application of bulk high-T_c cuprate superconductors. The above problem exists in almost all cuprate superconductors, such as YBCO, BSCCO, and Cu-1234. polycrystalline sample[42]. Therefore, improving or eliminating the weak link problem constitutes further work needed for Cu-1234 polycrystalline samples.

Conclusion

The cuprate superconductor Cu-1234, which is synthesized under high oxygen pressure, has a high T_c (~117 K) with a high J_c (>10^4 A/cm^2, 100 K), even in a heavily overdoped state; thus, it provides great potential for application above the liquid nitrogen temperature. The atomic-scale structure and electronic structure of Cu-1234 were revealed to underlie the observed excellent "double high" performance by using a series of techniques based on aberration-corrected STEM. A clear $\boldsymbol{a}\times2\boldsymbol{b}\times2\boldsymbol{c}$ modulated structure and plate-like microdomains inside the crystal have been commonly observed and are well interpreted by ordering of copper and oxygen vacancies in CRBs. Careful investigation of the alterations in the local atomic structure revealed the strong structural effects of periodic copper and oxygen deficiencies on the basic lattice. These structural features are thought to introduce pinning centers into the crystals, which evidently suppress vortex flux flow and enhance the critical current density. The symmetry and distribution of holes in Cu-1234, which provide a suitable electronic structure for high-J_c, were further explored with orientation-dependent EELS and EELS-STEM at atomic resolution. The "intrinsic" high-J_c of Cu-1234 at the liquid nitrogen temperature originate from its composition and crystal structure. The charge-reservoir blocks [$Ba_2CuO_{3+\delta}$] with rare compressed [CuO_6] octahedra and metallic conductivity give rise to many holes having p_z symmetry, which decreases the superconducting anisotropy and enhances the interlayer coupling that guarantees a high-J_c. A high carrier concentration in a high-T_c superconductor is essential for high J_c. The inhomogeneous carrier distribution in thick superconducting layers [$Ca_3Cu_4O_8$], with OP overdoping and IPs exhibiting near-optimal doping, maintains the high T_c of approximately 117 K even in a heavily overdoped state, which provides the necessary conditions for coexistence of high T_c and high J_c. Our results are applicable to design and synthesis of new multilayered superconductors with high T_c as well as high J_c.

Acknowledgements

This work was financially supported by the Chinese National Natural Science Foundation (Basic Science Center Project of NSFC under grant Nos. 51788104, 51527803, 11834009). Thanks to Ji Hua Laboratory Project X210141TL210 for cooperation. This work made use of the resources of the National Center for Electron Microscopy in Beijing. We acknowledge support from the Max Planck-POSTECH-Hsinchu Center for Complex Phase Materials.

Author details

[1]National Center for Electron Microscopy in Beijing, School of Materials Science and Engineering, Key Laboratory of Advanced Materials (MOE), The State Key Laboratory of New Ceramics and Fine Processing, Tsinghua University, Beijing 100084, China. [2]Ji Hua Laboratory, Foshan 528299, China. [3]Beijing National Laboratory for Condensed Matter Physics and Institute of Physics, Chinese Academy of Sciences, Beijing 100190, China. [4]Spallation Neutron Source Science Center, Dongguan 523803, China. [5]Max Planck Institute for Chemical Physics of Solids, Nöthnitzer Straβe 40, Dresden 01187, Germany

Author contributions

X.Z. and J.F.Z. contributed equally to this work. X.Z., J.C., and J.Z. proposed and designed the research. X.Z. and H.Z. carried out the TEM/STEM characterizations; J.F.Z. and L.S. fabricated the Cu-1234 samples and performed the magnetic property measurements; S.D., J.C., and L.H. performed the neutron powder diffraction experiments; Z.H. performed the neutron powder diffraction and soft X-ray absorption spectroscopy experiments. X.Z. and H.Z. analyzed the data and wrote the paper and Supplementary Information. All authors discussed the results and approved the final version of the manuscript.

Conflict of interest

The authors declare no competing interests.

Supplementary information The online version contains supplementary material available at https://doi.org/10.1038/s41427-022-00396-2.

Received: 29 December 2021 Revised: 23 April 2022 Accepted: 27 April 2022
Published online: 10 June 2022

References

1. Blatter, G., Feigel'man, M. V., Geshkenbein, V. B., Larkin, A. I. & Vinokur, V. M. Vortices in high-temperature superconductors. *Rev. Mod. Phys.* **66**, 1125–1388 (1994).
2. Bishop, D. J., Gammel, P. L., Huse, D. A. & Murray, C. A. Magnetic flux-line lattices and vortices in the copper oxide superconductors. *Science* **255**, 165–172 (1992).
3. Ricketts, J., Puzniak, R., Liu, C.-J., Gu, G. D., Koshizuka, N. & Yamauchi, H. Anisotropy and irreversibility line of iodine intercalated $Bi_2Sr_2CaCu_2O_{8+\delta}$ single crystals. *Appl. Phys. Lett.* **65**, 3284–3286 (1994).
4. Chong, I. et al. High critical-current density in the heavily Pb-doped $Bi_2Sr_2CaCu_2O_{8+\delta}$ superconductor: Generation of efficient pinning centers. *Science* **276**, 770–773 (1997).
5. Karppinen, M. & Yamauchi, H. Control of the charge inhomogeneity and high-T_c superconducting properties in homologous series of multi-layered copper oxides. *Mat. Sci. Eng. R. Rep.* **26**, 51–96 (1999).
6. Patel, R. H., Nabialek, A. & Niewczas, M. Characterization of superconducting properties of BSCCO powder prepared by attrition milling. *Supercond. Sci. Technol.* **18**, 317–324 (2005).
7. Clayton, N., Musolino, N., Giannini, E., Garnier, V. & Flükiger, R. Growth and superconducting properties of $Bi_2Sr_2Ca_2Cu_3O_{10}$ single crystals. *Supercond. Sci. Technol.* **17**, S563–S567 (2004).
8. Fujinami, K., Suematsu, H., Karppinen, M. & Yamauchi, H. Effect of overdoping on the irreversibility field and critical current density of the $HgBa_2Ca_2Cu_3O_{8+\delta}$ superconductor. *Physica C* **307**, 202–208 (1998).
9. Zheng, D. N., Campbell, A. M., Liu, R. S. & Edwards, P. P. Critical current, magnetic irreversibility line and relaxation in a single Tl-O layer 1223 superconductor. *Cryogenics* **33**, 46–49 (1993).
10. Choi, K.-Y. et al. High and uniform critical current density for large-size $YBa_2Cu_3O_{7-\delta}$ single crystals. *Curr. Appl. Phys.* **11**, 1020–1023 (2011).
11. Daeumling, M., Seuntjens, J. M. & Larbalestier, D. C. Oxygen-defect flux pinning, anomalous magnetization and intra-grain granularity in $YBa_2Cu_3O_{7-\delta}$. *Nature* **346**, 332–335 (1990).
12. Dou, S. X. et al. Enhancement of the critical current density and flux pinning of MgB_2 superconductor by nanoparticle SiC doping. *Appl. Phys. Lett.* **81**, 3419–3421 (2002).
13. Dolan, G. J., Chandrashekhar, G. V., Dinger, T. R., Feild, C. & Holtzberg, F. Vortex structure in $YBa_2Cu_3O_7$ and evidence for intrinsic pinning. *Phys. Rev. Lett.* **62**, 827–830 (1989).
14. Daeumling, M., Seuntjens, J. M. & Larbalestier, D. C. Oxygen-defect flux pinning, anomalous magnetization and intra-grain granularity in $YBa_2Cu_30_{7-\delta}$. *Nature* **346**, 332–335 (1990).
15. Civale, L. Vortex pinning and creep in high-temperature superconductors with columnar defects. *Supercond. Sci. Technol.* **10**, A11–A28 (1997).
16. Deutscher, G. Impact of pseudo-gap states on the pinning energy and irreversibility field of high temperature superconductors. *APL Mater.* **2**, 096108 (2014).
17. Shimoyama, J.-i Generic guiding law between irreversibility field and anisotropy-chemical control of critical current of high temperature superconductors. *J. Low. Temp. Phys.* **131**, 1043–1052 (2003).
18. Jin, C. Q., Adachi, S., Wu, X. J., Yamauchi, H. & Tanaka, S. 117 K superconductivity in the Ba–Ca–Cu–O system. *Physica C* **223**, 238–242 (1994).
19. Zhao, J., Li, W. & Jin, C. Composition simple and environmental friendly high temperature cuprate superconductors: Cu12(n−1)n. *Sin.-Phys. Mech. Astron* **48**, 087405 (2018).
20. Christen, D. K. & Thompson, R. Current problems at high T_c. *Nature* **364**, 98–99 (1993).
21. Iyo, A., Tokiwa, K., Terada, N., Tokumoto, M., Hirabayashi, M. & Ihara, H. Critical current density and irreversibility line of $CuBa_2Ca_3Cu_4O_y$. *Adv. Cryog. Eng.* **42**, 623–628 (1997).
22. Toby, B. H. EXPGUI, a graphical user interface for GSAS. *J. Appl. Crystallogr.* **34**, 210–213 (2001).
23. Jin, C. Q., Qin, X. M., Shimizu, K., Nishiyama, M., Namiki, T. & Yu, Y. The enhanced superconductivity of Cu-1234 under high pressure. *Int. J. Mod. Phys. B* **19**, 335–337 (2012).
24. Antipov, E. V. et al. The synthesis and characterization of the $HgBa_2Ca_2Cu_3O_{8+\delta}$ and $HgBa_2Ca_3Cu_4O_{10+\delta}$ phases. *Physica C* **215**, 1–10 (1993).
25. Ihara, H. et al. Crystal structure of a new high-T_c $TlBa_2Ca_3Cu_4O_{11}$ superconductor by high-resolution electron microscopy. *Phys. Rev. B Condens. Matter* **38**, 11952–11954 (1988).
26. Chen, C. T. et al. Out-of-plane orbital characters of intrinsic and doped holes in $La_{2-x}Sr_xCuO_4$. *Phys. Rev. Lett.* **68**, 2543–2546 (1992).
27. Tjeng, L. H., Chen, C. T. & Cheong, S. W. Comparative soft-X-ray resonant-photoemission study on $Bi_2Sr_2CaCu_2O_8$, CuO, and Cu_2O. *Phys. Rev. B Condens. Matter* **45**, 8205–8208 (1992).
28. Saini, N. L. et al. Polarized X-ray absorption spectroscopy study of the symmetry of unoccupied electronic states near the Fermi level in the $Bi_2Sr_2CaCu_2O_8$ system. *J. Phys.: Condens. Matter* **8**, 2467–2477 (1996).
29. Nücker, N. et al. Site-specific and doping-dependent electronic structure of $YBa_2Cu_3O_x$ probed by O 1s and Cu 2p X-ray-absorption spectroscopy. *Phys. Rev. B Condens. Matter* **51**, 8529–8542 (1995).
30. Li, W. M. et al. Superconductivity in a unique type of copper oxide. *Proc. Natl Acad. Sci. USA* **116**, 12156–12160 (2019).
31. Jin, C.-Q. et al. High-pressure synthesis and superconducting properties of the oxychloride superconductor$(Sr, Ca)_3Cu_2O_{4+\delta}Cl_{2-y}$. *Phys. Rev. B* **61**, 778–783 (2000).
32. Deutscher, G. & de Gennes, P.-G. A spatial interpretation of emerging superconductivity in lightly doped cuprates. *C. R. Phys.* **8**, 937–941 (2007).
33. Song, D. et al. Visualization of dopant oxygen atoms in a $Bi_2Sr_2CaCu_2O_{8+\delta}$ superconductor. *Adv. Funct. Mater.* **29**, 1903843 (2019).
34. Hÿtch, M. J., Snoeck, E. & Kilaas, R. Quantitative measurement of displacement and strain fields from HREM micrographs. *Ultramicroscopy* **74**, 131–146 (1998).
35. Kwok, W. K., Welp, U., Crabtree, G. W., Vandervoort, K. G., Hulscher, R. & Liu, J. Z. Direct observation of dissipative flux motion and pinning by twin boundaries in $YBa_2Cu_3O_{7-\delta}$ single crystals. *Phys. Rev. Lett.* **64**, 966–969 (1990).
36. Liu, J. et al. Boosting superconducting properties of Fe(Se, Te) via dual-oscillation phenomena induced by fluorine doping. *ACS Appl. Mater. Interfaces* **11**, 18825–18832 (2019).
37. Liu, J. et al. Synthesis of high-quality $FeSe_{0.5}Te_{0.5}$ polycrystal using an easy one-step technique. *J. Alloy. Compd.* **644**, 523–527 (2015).
38. Fink, J., Nücker, N., Pellegrin, E., Romberg, H., Alexander, M. & Knupfer, M. Electron energy-loss and X-ray absorption spectroscopy of cuprate superconductors and related compounds. *J. Electron Spectrosc. Relat. Phenom.* **66**, 395–452 (1994).
39. Nücker, N., Romberg, H., Xi, X. X. & Fink, J. Symmetry of holes in high-T_c superconductors. *Phys. Rev. B Condens. Matter* **39**, 6619–6629 (1989).
40. Pellegrin, E. et al. Polarized X-ray-absorption study of $Tl_2Ba_2CaCu_2O_8$ and $Tl_2Ba_2Ca_2Cu_3O_{10}$. *Phys. Rev. B Condens. Matter* **48**, 10520–10523 (1993).
41. Brown, I. D. & Altermatt, D. Bond-valence parameters obtained from a systematic analysis of the inorganic crystal structure database. *Acta Crystallogr., Sect. B: Struct. Sci.* **41**, 244–247 (1985).
42. Hilgenkamp, H. & Mannhart, J. Grain boundaries in high-T_c superconductors. *Rev. Mod. Phys.* **74**, 485–549 (2002).
43. Stöhr, J. NEXAFS spectroscopy. *Springe. Ser. Surf. Sci.* **25**, 211–231 (1996).